Supporting Information

Hydrophobic Layer of Amino Acid Enabling Dendrite-free Zn Anode for Aqueous Zinc-ion Batteries

Qing Wen[1,2], Hao Fu[1,2], Zhen-yu Wang[1,2], Ying-de Huang[1,2], Zhen-jiang He[1,2], Cheng Yan[3], Jing Mao[4], Kehua Dai[5], Xia-hui Zhang[6*], Jun-chao Zheng[1,2*]

[1]School of Metallurgy and Environment, Central South University, Changsha, Hunan, 410083, China

[2]Engineering Research Center of the Ministry of Education for Advanced Battery Materials, Central South University, Changsha 410083, China

[3]School of Mechanical, Medical and Process Engineering, Queensland University of Technology, Brisbane, Queensland, 4001, Australia

[4]School of Materials Science and Engineering, Zhengzhou University, Zhengzhou 450001, China.

[5]College of Chemistry, Tianjin Normal University, Tianjin 300387, China.

[6]School of Mechanical and Materials Engineering, Washington State University, Pullman, Washington 99164, United States

Corresponding Authors: xiahui.zhang@wsu.edu(X.h.Zhang), jczheng@csu.edu.cn (j. c. Zheng)

1.1 Experimental Section

Synthesis of δ-MnO_2 for cathode: The δ-MnO_2 was synthesized by hydrothermal synthesis.[1] In detail, 2.8446 g of $KMnO_4$ and 0.5070g of $MnSO_4 \cdot H_2O$ were added separately to 30 mL of DI water, followed by magnetically stirring for 30 minutes. Then, $KMnO_4$ solution (0.6 M) was mixed with $MnSO_4$ solution (0.1 M) under continuous stirring for 1 h at room temperature. The mixture was then transferred to a 100 mL Teflon-lined autoclave and maintained at 140 ℃ for 14 hours. The obtained brown solid product was centrifuged, and washed with DI water until the centrifuged solution was colourless, and then washed once with alcohol. Finally, the solid was dried in the oven at 80 ℃ overnight.

The δ-MnO_2 cathode was prepared by mixing 80 wt% of δ-MnO_2, 10 wt% of acetylene black, and 10 wt% of PVDF in NMP solution. The obtained slurry mixture was coated on carbon paper, followed by drying at 60℃ overnight in the vacuum oven. Finally, carbon paper loaded with δ-MnO_2 was cut into discs with a dimeter of 12 mm (loading of 1.5-2.5 mg).

Materials characterization: The surface morphologies and compositions of all zinc foil were investigated by field emission scanning electron microscopy (SEM, JSM-7900F) with an X-ray energy spectrum (EDS) detectors. The composition of the cathode material and the crystalline structure of the zinc foil were analysed by X-ray diffraction (XRD, PANalytical/ Empyrean 2). The chemical composition of the surface of zinc foil was characterized by the X-ray photoelectron spectroscopy (XPS, Thermo Scientific K-Alpha). The dynamic contact angles were measured by a contact angle sensors (LAUDA Scientific GmbH, LSA-100) to evaluate the wettability of zinc foil.

Theoretical calculations: All the DFT calculations were performed in Gaussian (G16)[2] program. The initial structures were optimized at the B3LYP/6-31+G(d,p) level of thoetry, followed by energy calcualtion at the B3LYP/6-311++G(2df,2p) level of thoetry, both with DFT-D3(BJ) dispersion correction.[3-7] The binding energy (ΔE) between two components was defined as following: $\Delta E = E_{total} - (E_A + E_B)$, where E_{total}, E_A, and E_B are the total energy of the A–B complexes, A component, and B component,

respectively. Here, A and B can be Zn ion, Cys anion, and H_2O.

Electrochemical Measurement: For symmetric cells, 2032-type coin cells were assembled. Bare Zn or Cys-Zn@Zn disc (16 mm) was used as working electrodes, glass fiber (GF/D) was used as separator, and 80 μL of $ZnSO_4$ (2 mol L^{-1}) aqueous solution was used as the electrolyte. The half coin cells were similar to the symmetric cells, but a 12-mm Cu foil replaced Bare Zn or Cys-Zn@Zn as counter electrode. In the full coin cells, the δ-MnO_2 cathode and Bare Zn or Cys-Zn@Zn anode were used, and 80 μL of mixed solution of $ZnSO_4$ (2 mol L^{-1}) and $MnSO_4$ (0.1 mol L^{-1}) was used as electrolyte. All of the cells were assembled in the atmospheric environment.

Galvanostatic cycling tests were carried out by the LAND CT2001A (Wuhan LAND electronics Co., Ltd.). CHI 660e electrochemical workstation (ChenHua Instruments Co., Ltd.) was used to record cyclic voltammetry (CV) curves of half coin cells (range of -0.3 to 1.0 V, scan rate of 5 mV s^{-1}) and full coin cells (range of 0.6 to 1.8V, scan rate of 0.2 mV s^{-1}), electrochemical impedance spectroscopy (EIS) spectra between 0.01 Hz and 100 kHz, and Tafel curves (range of -0.3 to 0.3V). The dendrite growth was observed by the in-situ optical microscopy (10XB-PC, Shang Guang) at the electricity of 5 mA.

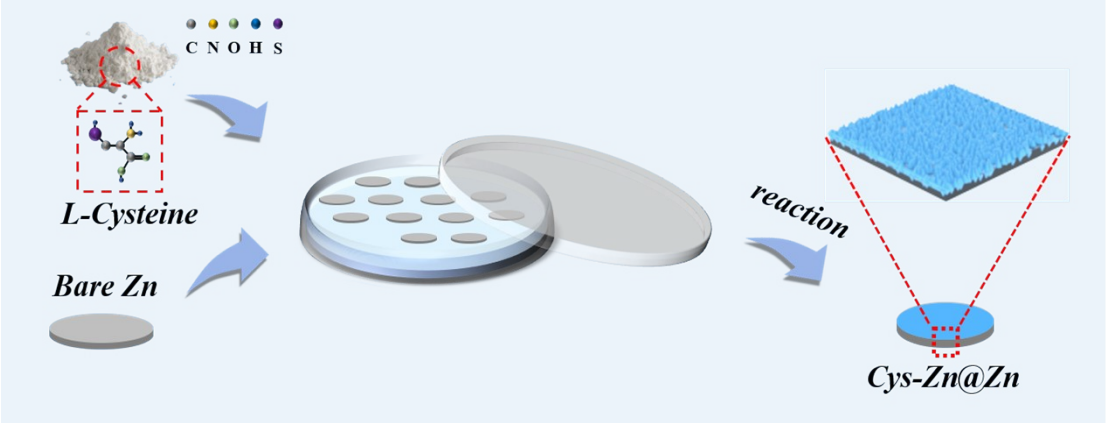

Figure S1. Schematic illustration of fabricating ultrathin L-cysteine complex layers on the Zn foil (Cys-Zn@Zn).

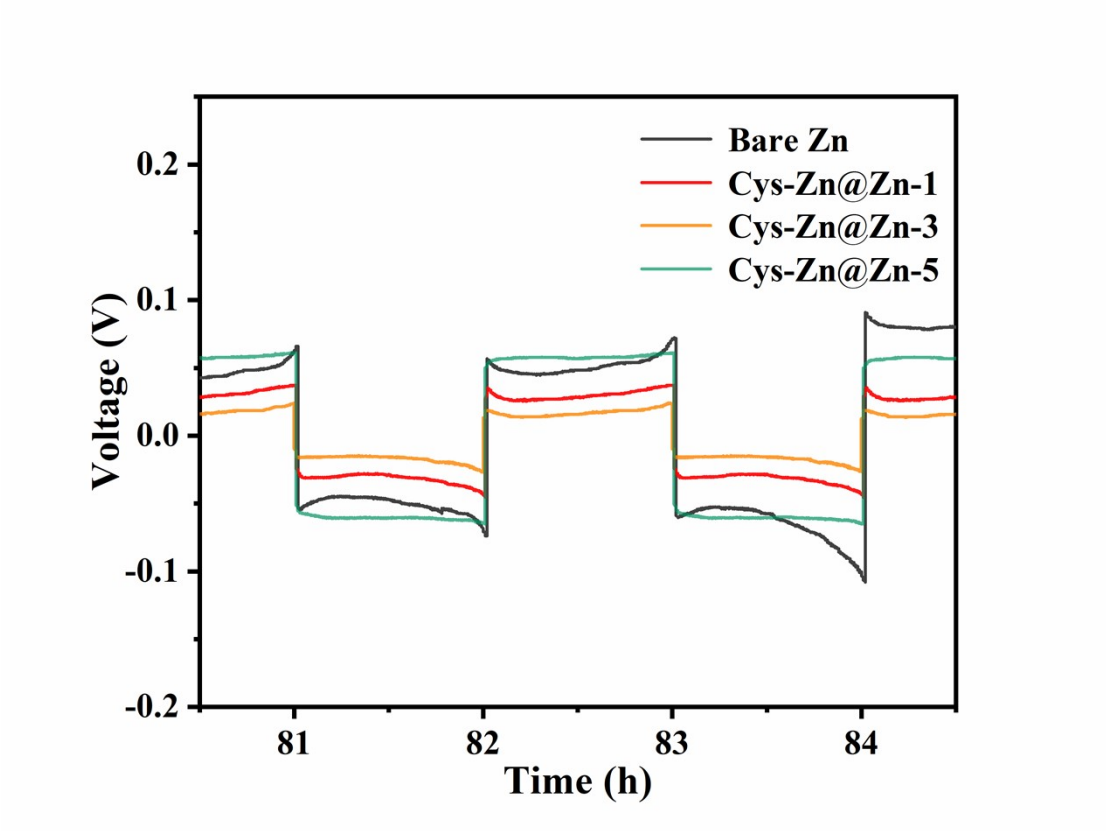

Figure S2. Partially scale cycling performance at selected cycles of Cys-Zn@Zn-x and Bare Zn symmetric cells for 2 mAh cm^{-2} at 2 mA cm^{-2}.

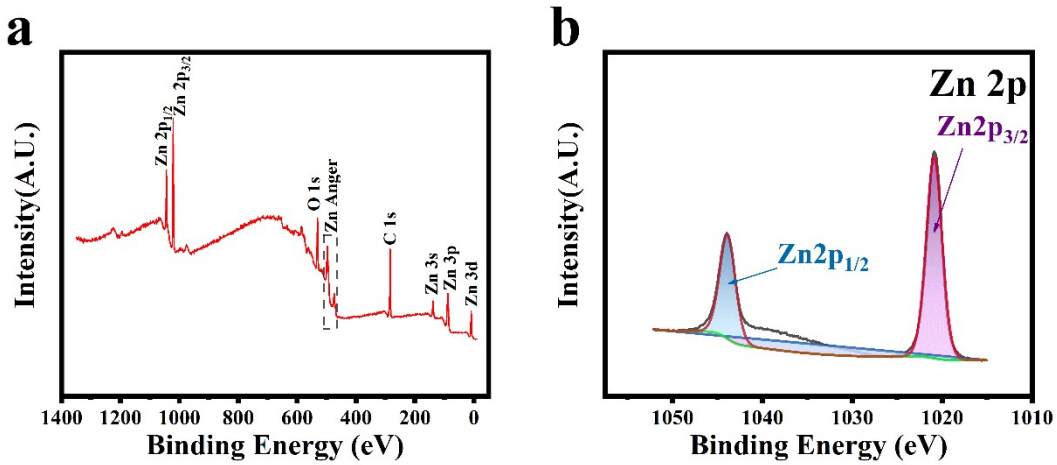

Figure S3. (a) The XPS survey spectra for Bare Zn. (b) Zn 2p XPS spectrum of Bare Zn.

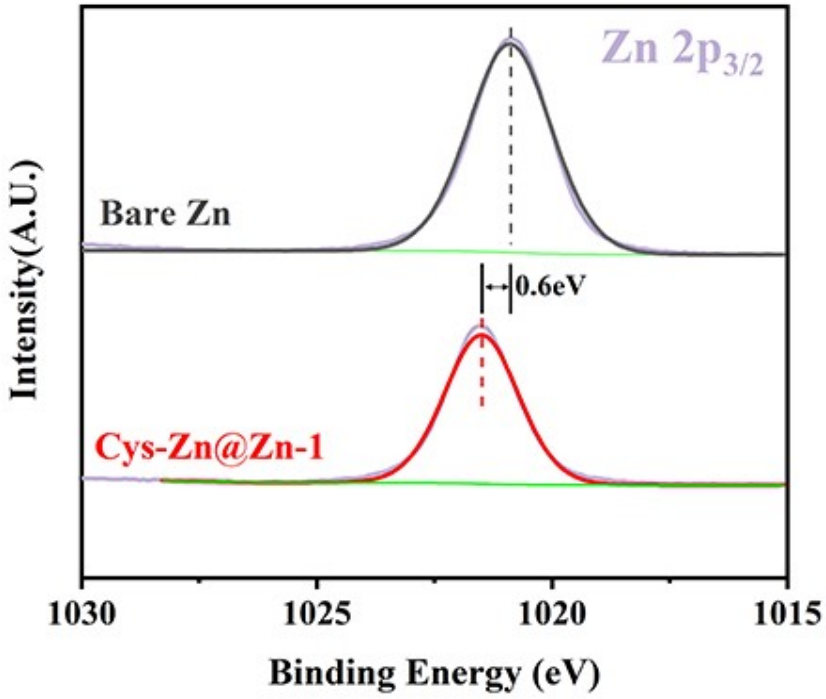

Figure S4. Partially scale Zn 2p XPS spectrum of Bare Zn (black) and Cys-Zn@Zn-1 (red).

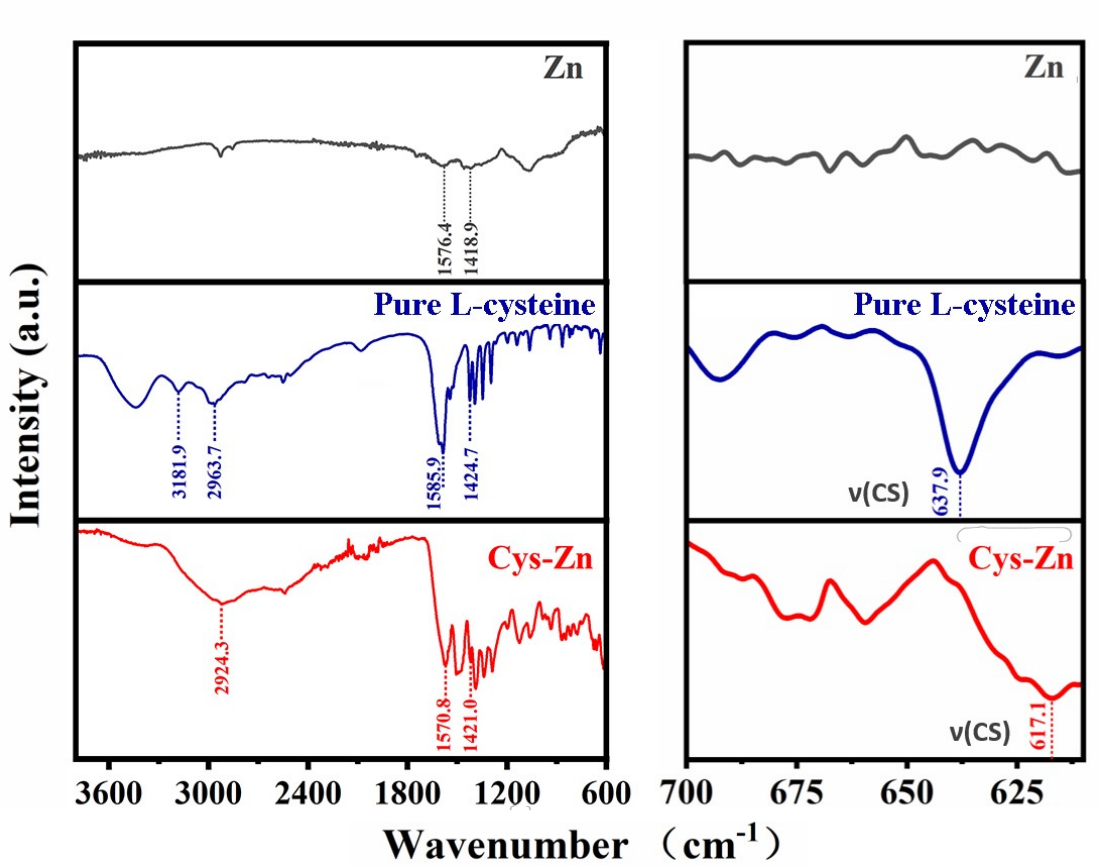

Figure S5. FTIR spectra and partially scale spectra at selected wavenumber of Zn, pure cysteine and Cys-Zn.

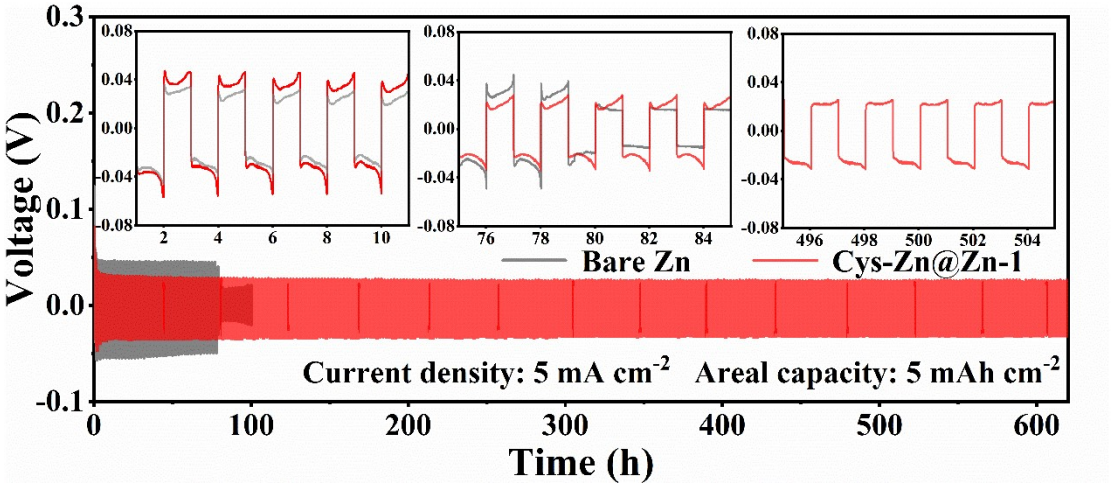

Figure S6. Cycling performance and partially scale voltage profiles at selected cycles of the Bare Zn and Cys-Zn@Zn-1 symmetric cells for 5 mAh cm^{-2} at 5 mA cm^{-2}.

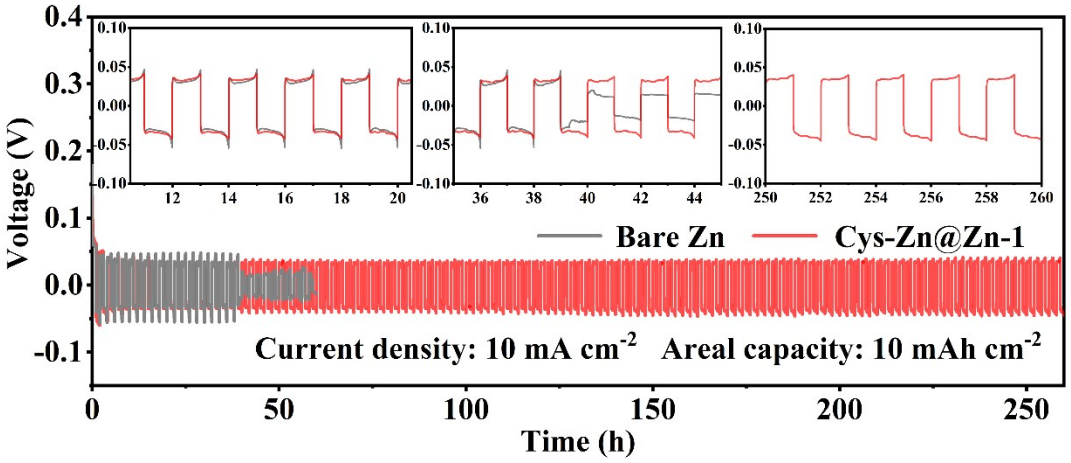

Figure S7. Cycling performance and Partially scale voltage profiles at selected cycles of the Bare Zn and Cys-Zn@Zn-1 symmetric cells for 10 mAh cm^{-2} at 10 mA cm^{-2}.

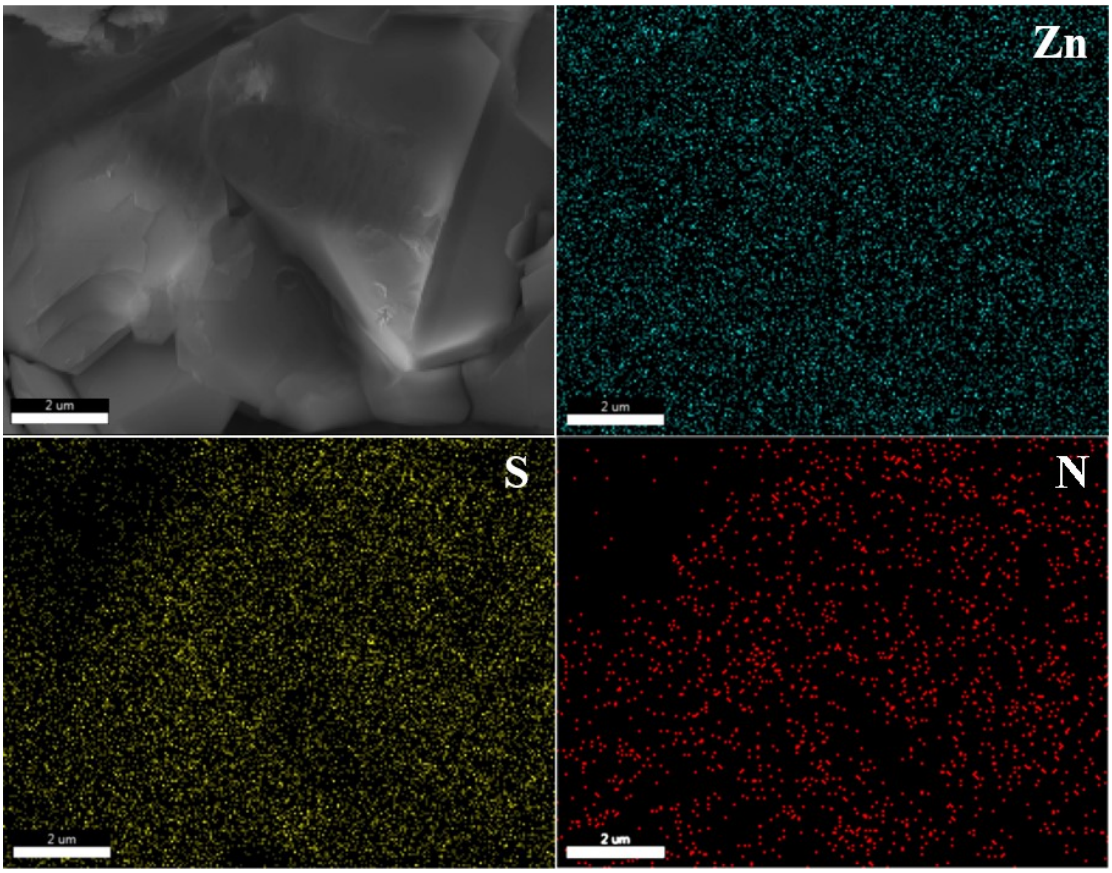

Figure S8. SEM pictures and the respective elemental profiles of the Cys-Zn@Zn-1 anode after 25 cycles at 2 mA cm^{-2} and 1 mAh cm^{-2}.

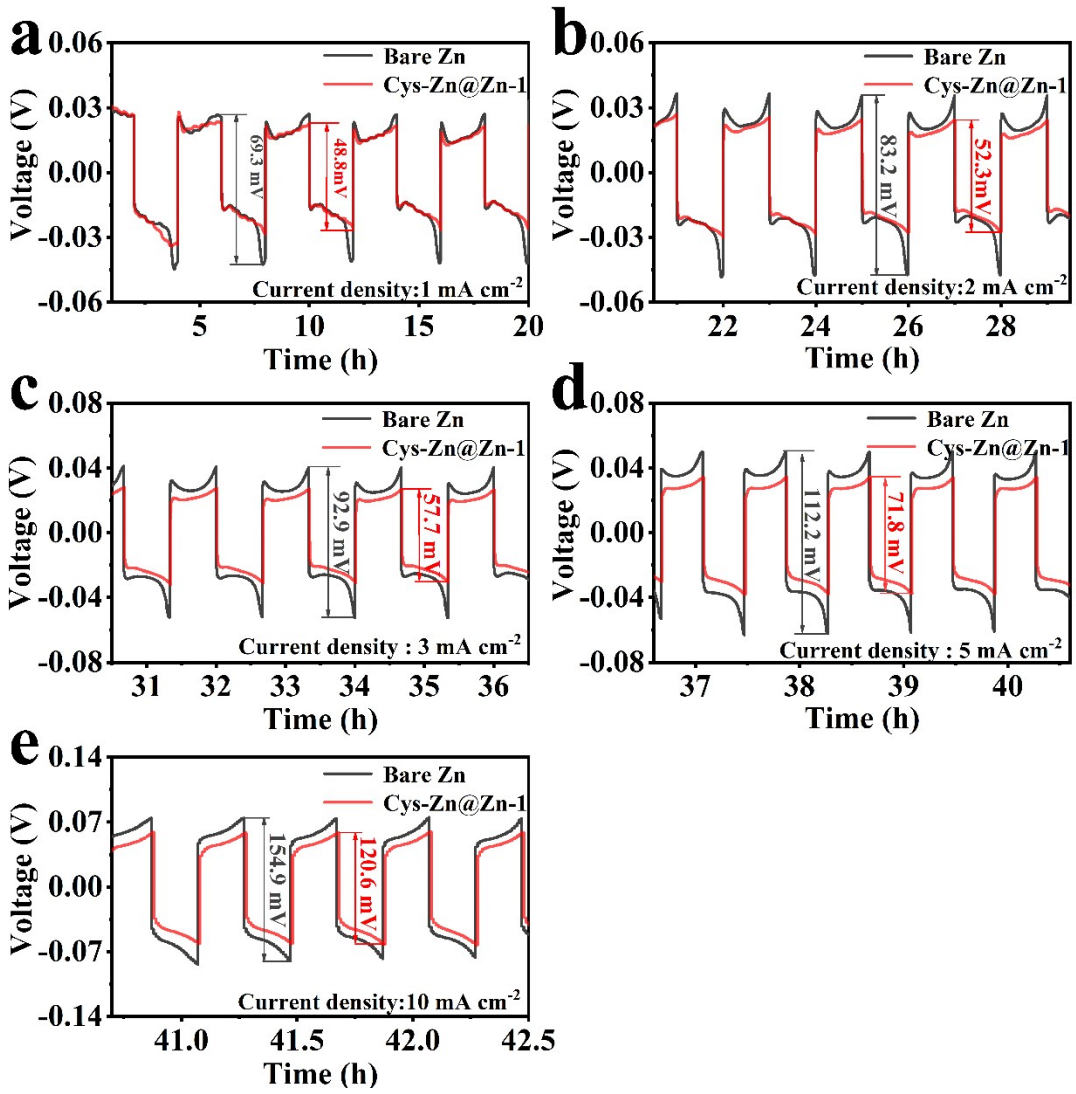

Figure S9. (a-e) Partially scale rate performance at selected cycles of Cys-Zn@Zn-1 and Bare Zn symmetric cells at (a) 1 mA cm^{-2}, (b) 2 mA cm^{-2}, (c) 3 mA cm^{-2}, (d) 5 mA cm^{-2} and (e) 10 mA cm^{-2} for 2 mAh cm^{-2}.

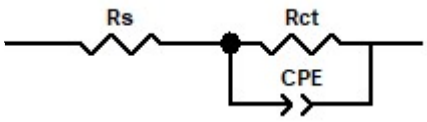

Figure S10. The equivalent circuits used for fitting the experimental spectra of Bare Zn and Cys-Zn@Zn-1 symmetric cells. Rs and Rct are denoted as electrolyte resistance, and interfacial resistance, respectively.

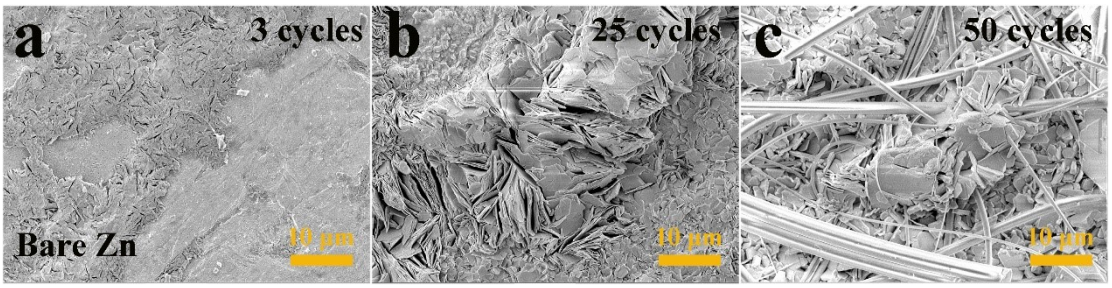

Figure S11. (a-c) SEM of the Bare Zn anode after plating/stripping (a) 3 cycles, (b) 25cycles and (c) 50 cycles for 1 mAh cm^{-2} at 2 mA cm^{-2}.

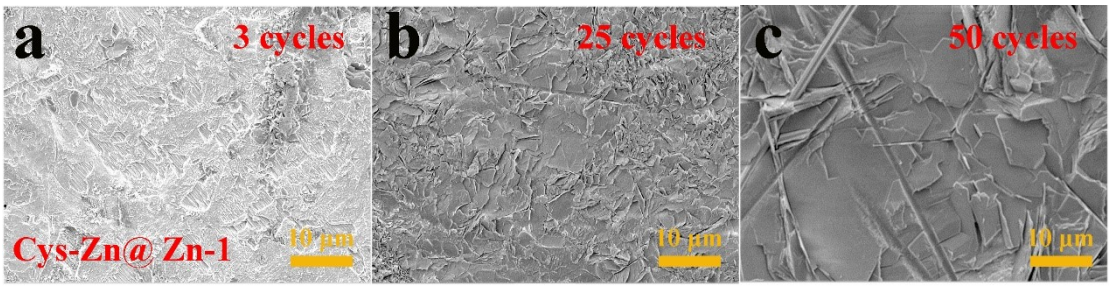

Figure S12. (a-c) SEM of the Cys-Zn@Zn-1 anode after plating/stripping (a) 3 cycles, (b) 25cycles and (c) 50 cycles for 1 mAh cm^{-2} at 2 mA cm^{-2}..

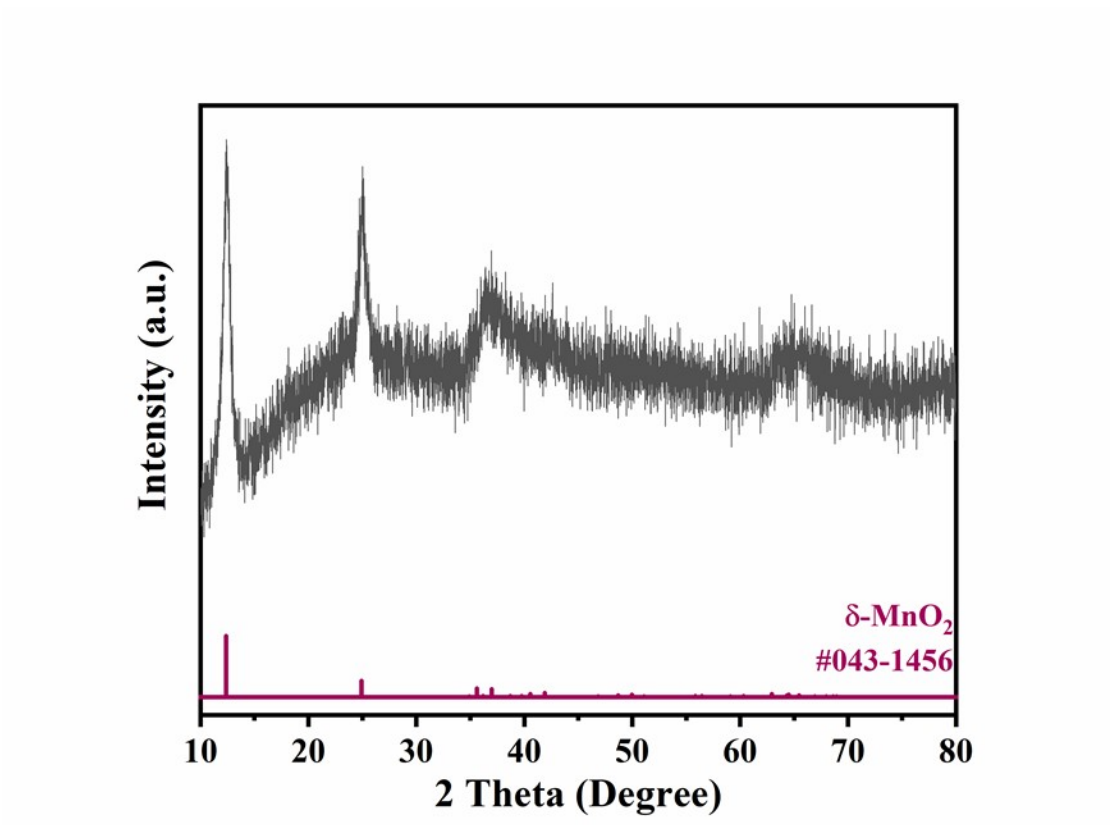

Figure S13. XRD pattern of MnO_2 showing the δ-MnO_2 structure (PDF: #043-1456)

Due to the low cost, high operating voltage and theoretical specific capacity,

especially MnO_2, manganese-based materials have a practical application prospect in zinc ion batteries. Referring to previous work, a simple hydrothermal method was employed to prepare δ-MnO_2. XRD was used to investigate the crystal structure of δ-MnO_2 samples with the peak corresponding to ICDD crystallographic database entry PDF#043-1456 , proving no other impurities[1] **(Figure S13)**.

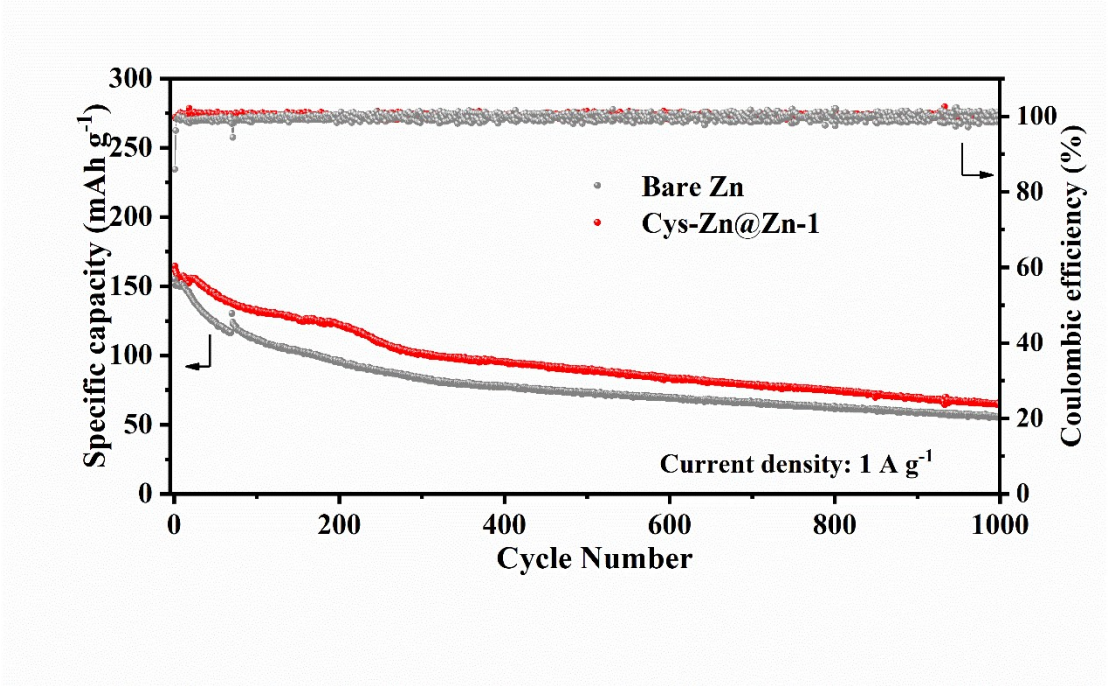

Figure S14. Long-term cycling performance of Zn||MnO_2 battery with Bare Zn and Cys-Zn@Zn-1 anodes at 1 A g^{-1} together with corresponding CEs.

Table S1. Ccomparison of this work with other previously reported cycling performance of symmetrical cells

Anodes	Areal capacity (mAh cm^{-2})	Current density (mA cm^{-2})	Cycle life (hour)	reference
S/MX@ZnS@Zn-350	0.5	0.5	1600	8
	1	1	1100	
	5	5	400	
Zn@ZnP	0.5	2	3300	9
	1.25	5	3200	
	2.5	10	1900	
Zn@N-VG@CC	0.5	0.5	150	10
	1	1	65	
NLSG coated Zn	1	1	250	11
Zn-ZnF_2	0.5	0.5	700	12
GFA-5	1	1	2000	13
	3	3	700	
Zn@ZIF	1	2	1100	14
	2	2	700	
	5	5	400	
	2.5	5	900	
DIP D@Zn	1	1	420	1
	1	2	260	
PPZ@Zn	0.5	1	3000	15
	1	1	350	
	1	2	600	
SEI-Zn	0.5	1	2500	16
	1	2	1900	
	2.5	5	600	
	5	10	450	
SLM-Zn	2	1	500	17
Zn@ZnO-3D	1.25	5	500	18
Zn@ZnF_2	1	1	800	19
	1	10	500	
502-coated Zn	0.25	0.5	800	20
N-C networks coated Zn foil	1	1	1020	21
	2	2	800	
	4	4	300	
Cys-Zn@Zn-1	**2**	**2**	**2000**	**This work**
	1	**2**	**2000**	
	5	**5**	**600**	
	10	**10**	**260**	

Table S2. The impedance parameters for bare Zn and Cys-Zn@Zn-1 in the initial, 3rd, 25th and 50th cycle.

	Bare Zn				Cys-Zn@Zn-1			
	Initial	3rd	25th	50th	Initial	3rd	25th	50th
R_s/Ω	0.926	1.905	1.403	1.019	0.818	2.105	1.305	1.446
R_{ct}/Ω	469.7	165.2	70.04	67.29	291.3	78.8	39.34	36.46

References

1. Park, J. H.; Kwak, M. J.; Hwang, C.; Kang, K. N.; Liu, N.; Jang, J. H.; Grzybowski, B. A., Self-Assembling Films of Covalent Organic Frameworks Enable Long-Term, Efficient Cycling of Zinc-Ion Batteries. *Adv Mater* **2021,** *33* (34), e2101726.

2. Frisch, M.; Trucks, G.; Schlegel, H.; Scuseria, G.; Robb, M.; Cheeseman, J.; Scalmani, G.; Barone, V.; Petersson, G.; Nakatsuji, H., Gaussian 16. Gaussian, Inc. Wallingford, CT: 2016.

3. Hehre, W. J.; Ditchfield, R.; Pople, J. A., Self—Consistent Molecular Orbital Methods. XII. Further Extensions of Gaussian—Type Basis Sets for Use in Molecular Orbital Studies of Organic Molecules. *The Journal of Chemical Physics* **1972,** *56* (5), 2257-2261.

4. Krishnan, R.; Binkley, J. S.; Seeger, R.; Pople, J. A., Self-consistent molecular orbital methods. XX. A basis set for correlated wave functions. *The Journal of Chemical Physics* **1980,** *72* (1), 650-654.

5. Lee, C.; Yang, W.; Parr, R. G., Development of the Colle-Salvetti correlation-energy formula into a functional of the electron density. *Physical Review B* **1988,** *37* (2), 785-789.

6. Caldeweyher, E.; Bannwarth, C.; Grimme, S., Extension of the D3 dispersion coefficient model. *The Journal of Chemical Physics* **2017,** *147* (3), 034112.

7. Becke, A. D., Density-functional thermochemistry. III. The role of exact exchange. *The Journal of Chemical Physics* **1993,** *98* (7), 5648-5652.

8. An, Y.; Tian, Y.; Liu, C.; Xiong, S.; Feng, J.; Qian, Y., Rational Design of Sulfur-Doped Three-Dimensional Ti3C2Tx MXene/ZnS Heterostructure as Multifunctional Protective Layer for Dendrite-Free Zinc-Ion Batteries. *ACS Nano* **2021,** *15* (9), 15259-15273.

9. Cao, P.; Zhou, X.; Wei, A.; Meng, Q.; Ye, H.; Liu, W.; Tang, J.; Yang, J., Fast-Charging and Ultrahigh-Capacity Zinc Metal Anode for High-Performance Aqueous Zinc-Ion Batteries. *Advanced Functional Materials* **2021,** *31* (20), 2100398.

10. Cao, Q.; Gao, H.; Gao, Y.; Yang, J.; Li, C.; Pu, J.; Du, J.; Yang, J.; Cai, D.; Pan, Z.; Guan, C.; Huang, W., Regulating Dendrite-Free Zinc Deposition by 3D Zincopilic Nitrogen-Doped Vertical Graphene for High-Performance Flexible Zn-Ion Batteries. *Advanced Functional Materials* **2021,** *31* (37), 2103922.

11. Guo, J.; Zhang, W.; Yin, J.; Zhu, Y.; Mohammed, Z. O. F.; Alshareef, H. N., Zincophilic Laser-Scribed Graphene Interlayer for Homogeneous Zinc Deposition and Stable Zinc-Ion Batteries. *Energy Technology* **2021,** *9* (10), 2100490.

12. Han, J.; Euchner, H.; Kuenzel, M.; Hosseini, S. M.; Groß, A.; Varzi, A.; Passerini, S., A Thin and Uniform Fluoride-Based Artificial Interphase for the Zinc Metal Anode Enabling Reversible Zn/MnO2 Batteries. *ACS Energy Letters* **2021,** *6* (9), 3063-3071.

13. Liang, G.; Zhu, J.; Yan, B.; Li, Q.; Chen, A.; Chen, Z.; Wang, X.; Xiong, B.; Fan, J.; Xu, J.; Zhi, C., Gradient fluorinated alloy to enable highly reversible Zn-metal anode chemistry. *Energy & Environmental Science* **2022,** *15*, 1086-1096.
14. Liu, X.; Yang, F.; Xu, W.; Zeng, Y.; He, J.; Lu, X., Zeolitic Imidazolate Frameworks as Zn(2+) Modulation Layers to Enable Dendrite-Free Zn Anodes. *Adv Sci (Weinh)* **2020,** *7* (21), 2002173.
15. Wang, X.; Meng, J.; Lin, X.; Yang, Y.; Zhou, S.; Wang, Y.; Pan, A., Stable Zinc Metal Anodes with Textured Crystal Faces and Functional Zinc Compound Coatings. *Advanced Functional Materials* **2021**, 2106114.
16. Di, S.; Nie, X.; Ma, G.; Yuan, W.; Wang, Y.; Liu, Y.; Shen, S.; Zhang, N., Zinc anode stabilized by an organic-inorganic hybrid solid electrolyte interphase. *Energy Storage Materials* **2021,** *43*, 375-382.
17. Wu, S.; Zhang, S.; Chu, Y.; Hu, Z.; Luo, J., Stacked Lamellar Matrix Enabling Regulated Deposition and Superior Thermo-Kinetics for Advanced Aqueous Zn-Ion System under Practical Conditions. *Advanced Functional Materials* **2021**, 2107397.
18. Xie, X.; Liang, S.; Gao, J.; Guo, S.; Guo, J.; Wang, C.; Xu, G.; Wu, X.; Chen, G.; Zhou, J., Manipulating the ion-transfer kinetics and interface stability for high-performance zinc metal anodes. *Energy & Environmental Science* **2020,** *13* (2), 503-510.
19. Yang, Y.; Liu, C.; Lv, Z.; Yang, H.; Zhang, Y.; Ye, M.; Chen, L.; Zhao, J.; Li, C. C., Synergistic Manipulation of Zn(2+) Ion Flux and Desolvation Effect Enabled by Anodic Growth of a 3D ZnF2 Matrix for Long-Lifespan and Dendrite-Free Zn Metal Anodes. *Adv Mater* **2021,** *33* (11), e2007388.
20. Cao, Z.; Zhu, X.; Xu, D.; Dong, P.; Chee, M. O. L.; Li, X.; Zhu, K.; Ye, M.; Shen, J., Eliminating Zn dendrites by commercial cyanoacrylate adhesive for zinc ion battery. *Energy Storage Materials* **2021,** *36*, 132-138.
21. Wu, C.; Xie, K.; Ren, K.; Yang, S.; Wang, Q., Dendrite-free Zn anodes enabled by functional nitrogen-doped carbon protective layers for aqueous zinc-ion batteries. *Dalton Trans* **2020,** *49* (48), 17629-17634.